nature chemical biology

ARTICLE

PUBLISHED ONLINE: 14 AUGUST 2017 | DOI: 10.1038/NCHEMBIO.2456

Optogenetic control of kinetochore function

Huaiying Zhang[1,3], Chanat Aonbangkhen[2,3], Ekaterina V Tarasovetc[1], Edward R Ballister[1], David M Chenoweth[2]* & Michael A Lampson[1]*

Kinetochores act as hubs for multiple activities during cell division, including microtubule interactions and spindle checkpoint signaling. Each kinetochore can act autonomously, and activities change rapidly as proteins are recruited to, or removed from, kinetochores. Understanding this dynamic system requires tools that can manipulate kinetochores on biologically relevant temporal and spatial scales. Optogenetic approaches have the potential to provide temporal and spatial control with molecular specificity. Here we report new chemical inducers of protein dimerization that allow us to both recruit proteins to and release them from kinetochores using light. We use these dimerizers to manipulate checkpoint signaling and molecular motor activity. Our findings demonstrate specialized properties of the CENP-E (kinesin-7) motor for directional chromosome transport to the spindle equator and for maintenance of metaphase alignment. This work establishes a foundation for optogenetic control of kinetochore function, which is broadly applicable to experimental probing of other dynamic cellular processes.

The kinetochore is a complex macromolecular structure, comprising of more than 100 different proteins, that assembles at the centromere of each chromosome during cell division[1,2]. Kinetochores perform multiple essential tasks for chromosome segregation, including building physical connections between chromatin and the force-generating microtubule (MT) polymers and housing regulatory proteins that ensure faithful segregation[3]. Defects in these processes lead to chromosome-segregation errors and genome instability, which are associated with cancer and developmental diseases[4]. Kinetochore function depends on the dynamic localization changes of components such as kinases, molecular motors and mitotic checkpoint proteins. For example, coordinated actions of plus- and minus-end-directed MT motors drive movement of chromosomes to align at the spindle equator[5,6] (**Fig. 1a**). This process of chromosome congression facilitates attachment of sister kinetochores to opposite spindle poles (bi-orientation), so that each daughter cell ultimately receives exactly one copy of each chromosome. Dynein initially transports chromosomes toward MT minus ends at spindle poles, and a kinesin-7 motor, centromere protein E (CENP-E), then transports them to MT plus ends at the spindle equator (**Fig. 1a**). The spindle checkpoint provides sufficient time for all chromosomes to congress and bi-orient by delaying anaphase in the presence of kinetochores lacking proper MT attachment[7,8]. Checkpoint signaling proteins are enriched on unattached kinetochores to activate the checkpoint and are released from attached kinetochores to silence the checkpoint (**Fig. 1a**). Each kinetochore can act autonomously, so that a single unattached kinetochore can signal the whole cell to wait before proceeding to anaphase. After congression and bi-orientation, kinetochores maintain stable attachments to dynamic microtubule plus ends, which ultimately drives chromosome segregation in anaphase (**Fig. 1a**).

A promising approach to understanding this complex and dynamic system is to manipulate kinetochores on biologically relevant temporal and spatial scales with molecular specificity, which has not been possible with existing methods. Molecular approaches such as genetic manipulations or RNA interference (RNAi) target specific proteins[9], but lack spatial and temporal control. Small-molecule inhibitors offer temporal, but not spatial, control, and their molecular specificity is variable and difficult to thoroughly characterize[10]. Laser microsurgery can be used to ablate single kinetochores with temporal control, but this method lacks molecular specificity[11].

Optogenetic tools have the potential to provide both spatiotemporal control and molecular specificity by using light and genetically encoded protein tags, respectively, and have emerged as important tools to probe dynamic cellular processes such as organelle transport, cell signaling and polarity[12–14]. We previously reported a photocaged chemical dimerizer that can recruit tagged proteins from the cytosol to multiple cellular structures[15,16]. Using this molecule, dimerization can be reversed by adding a competitor, but a major limitation of this is that reversal is slow and lacks spatial control. One feature of this system is the modular design of the dimerizer, which facilitates the development of new molecules on the same platform.

Here we exploit this design by developing two new dimerizers. One can be uncaged using less light and longer wavelengths. The other allows reversal of dimerization, so that proteins can be recruited to and subsequently released from cellular structures. We apply those dimerizers to manipulate two important kinetochore functions: checkpoint signaling and molecular motor activity. Overall, our findings establish a foundation for opotogenetic manipulation of kinetochores and reveal specialized properties of the motor protein CENP-E for transporting chromosomes specifically toward the spindle equator and stabilizing the metaphase plate.

RESULTS

New optogenetic tools

Our previously reported dimerizer, NTH (**1**), contains three modules: a 6-nitroveratryl oxycarbonyl (NVOC) photocage to prevent untargeted dimerization; trimethoprim (TMP), which noncovalently binds to *Escherichia coli* dihydrofolate reductase (eDHFR); and a Halo ligand that covalently binds to a bacterial alkyldehalogenase enzyme (referred to as Haloenzyme; **Fig. 1b**). Illumination removes the photocage, allowing dimerization of eDHFR-tagged proteins with Halo-tagged proteins. Based on this modular design, we developed two new dimerizers that offer additional properties: increased sensitivity to light and rapid light-induced reversal of dimerization.

[1]Department of Biology, School of Arts and Sciences, University of Pennsylvania, Philadelphia, Pennsylvania, USA. [2]Department of Chemistry, School of Arts and Sciences, University of Pennsylvania, Philadelphia, Pennsylvania, USA. [3]These authors contributed equally to this work.
*e-mail: lampson@sas.upenn.edu or dcheno@sas.upenn.edu

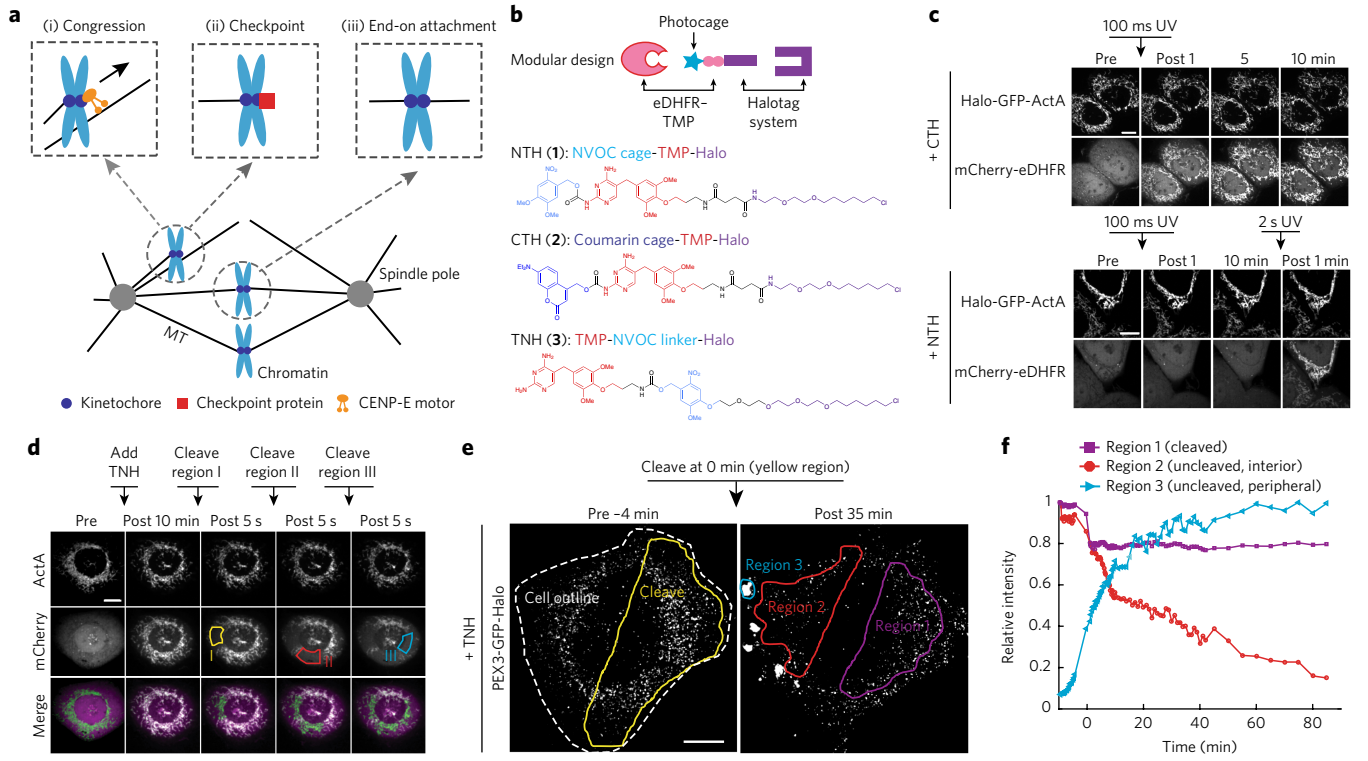

Figure 1 | New dimerizers based on a modular design. (**a**) Kinetochore functions in cell division. (i) Chromosome congression: CENP-E motors at kinetochores transport chromosomes to the spindle equator. (ii) Checkpoint signaling proteins localize to unattached kinetochores. (iii) Bi-oriented kinetochores maintain stable end-on MT attachment. MT, microtubule. (**b**) Optogenetic toolbox: NTH was previously published[15]; CTH uses a different photocage; TNH is photocleavable between TMP and Halo. eDHFR, *Escherichia coli* dihydrofolate reductase; TMP, trimethoprim; NVOC, 6-nitroveratryl oxycarbonyl. (**c**) Cells expressing mCherry-eDHFR and Halo-GFP-ActA, which localizes to mitochondria, were incubated with 10 μM CTH or NTH. Cells were illuminated with a 100-ms pulse of wide-field UV (387 ± 5 nm), which was sufficient to uncage CTH but not NTH, followed by a 2 s pulse to uncage NTH. (**d**) Cells expressing mCherry-eDHFR and Halo-GFP-ActA were incubated with 100 nM TNH to recruit mCherry to mitochondria. Three regions (outlined in yellow, red or blue) were illuminated sequentially with a 405-nm laser to cleave TNH and release mCherry from mitochondria. Merged images show Halo-GFP-ActA in green and mCherry-eDHFR in magenta. (**e**,**f**) Cells expressing kinesin light chain 1 (KLC1)-mCherry-eDHFR and PEX3-GFP-Halo, which localizes to peroxisomes, were treated with 100 nM TNH at $t = -4$ min to induce peroxisome transport toward the cell periphery. Half the cell (yellow region) was illuminated with a 405-nm laser at $t = 0$ to cleave TNH. GFP intensity was quantified (**f**) in the interior region (1), where TNH was cleaved, and in interior and peripheral regions (2 and 3, respectively) that were not exposed to 405 nm light. Intensity in each region over time is shown as a fraction of the maximal intensity in that region. Scale bars, 10 μm.

First, we replaced the NVOC with a [7-(diethylamino)-coumarin-4-yl]methyl (DEACM) photocage, which is more sensitive to light and can be uncaged at longer wavelengths[17]. Details of the synthetic scheme and characterization can be found in **Supplementary Note 1**. This new molecule, CTH (**2**) (**Fig. 1b**), enters living cells, as shown in cells expressing Haloenzyme fused to the centromere protein B (CENP-B) (**Supplementary Results**, **Supplementary Fig. 1a**), and is not toxic to cells at the concentrations used in our experiments (**Supplementary Fig. 1b**). To show that CTH can recruit proteins from the cytosol to cellular structures, we targeted mCherry to mitochondria by uncaging CTH with 385 nm light. Notably, CTH requires less light than NTH to uncage (**Fig. 1c**), and can also be uncaged with 444 nm light, whereas NTH is only sensitive to shorter wavelengths (**Supplementary Fig. 1c,d**).

Second, we developed a dimerizer that can be cleaved with light to reverse dimerization. Taking advantage of the modular design of our system, we inserted a cleavable NVOC linker in between the Halo and TMP ligands to make TNH (**3**) (**Fig. 1b**). Details of the synthetic scheme and characterization can be found in **Supplementary Note 1**. To show that TNH enters live cells and recruits proteins to cellular structures, we targeted mCherry-eDHFR to mitochondria. The kinetics of recruitment depend on TNH concentration (**Supplementary Fig. 1e**), with the highest degree of dimerization ($t_{1/2}$ ~2 min) observed at 0.1 μM. A higher concentration of TNH (1 μM) is less effective, because independent occupancy of both protein binding sites with two different TNH molecules would lead to unproductive protein–ligand complexes. A lower concentration (0.01 μM) required more time ($t_{1/2}$ ~5 min) to achieve maximum dimerization, which is ~80% of the maximum dimerization obtained with 0.1 μM. TNH is not toxic to cells at these concentrations (**Supplementary Fig. 1b**). To test whether the recruitment of proteins can be reversed with light, we targeted multiple regions sequentially with a 405-nm laser (**Fig. 1d**). mCherry was released rapidly in the illuminated regions, demonstrating reversal of dimerization with spatiotemporal control.

As a functional test of the new dimerizers, we used them to control organelle transport. We previously showed that recruitment of kinesin or dynein motors to peroxisomes induces transport to the periphery or center of the cell, respectively[16]. Recruiting the dynein adaptor Bicaudal-D (BICD) to peroxisomes by uncaging CTH led to peroxisome accumulation at the cell center, as expected (**Supplementary Fig. 2**). To show that transport can be halted by reversing dimerization, we used TNH to recruit an N-terminal fragment of kinesin light chain 1 (KLC1) to peroxisomes, and subsequently cleaved it with light on one side of the cell (**Fig. 1e**, yellow region). After incubation with TNH, but before cleavage,

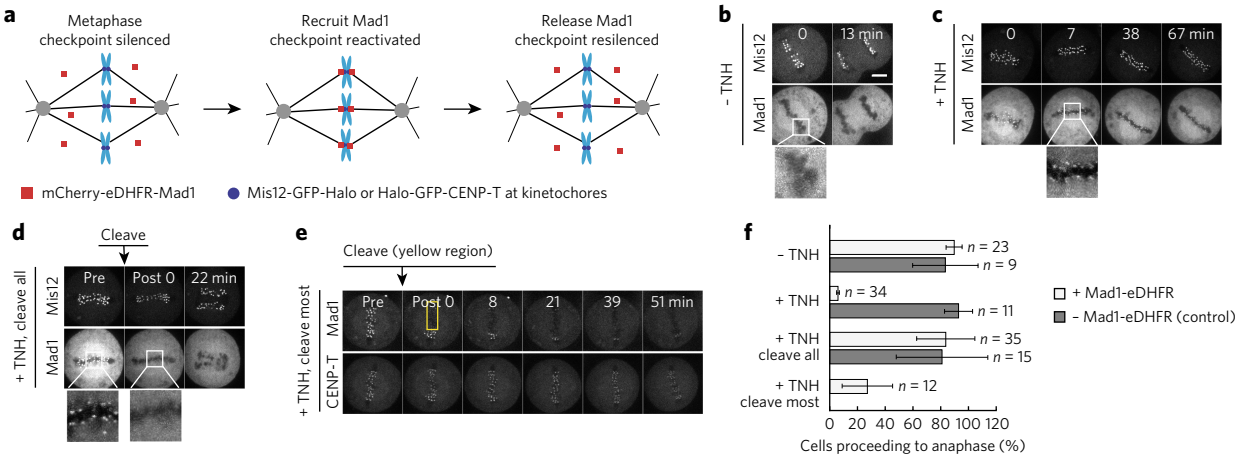

Figure 2 | Activating and silencing the spindle checkpoint. (**a**) Experimental design for cells expressing mCherry-eDHFR-Mad1 and either Mis12-GFP-Halo or Halo-GFP-CENP-T. (**b**) Control experiment: with no TNH treatment and no Mad1 recruitment to metaphase kinetochores, cells proceeded to anaphase normally. (**c**–**f**) With treatment of 100 nM TNH, eDHFR-Mad1 was recruited to metaphase kinetochores. (**c**) Without cleavage cells arrested in metaphase. (**d**) TNH cleavage over the whole cell at $t = 0$ released Mad1 from all kinetochores, and cells proceeded to anaphase. Insets (white boxes) are magnified for visualization. (**e**) TNH cleavage in a region covering most of the metaphase plate (yellow rectangle) released Mad1 from kinetochores in this region, and cells arrested in metaphase. (**f**) The percentage of cells entering anaphase within 30 min under the indicated conditions was quantified for cells with or without eDHFR-Mad1. Error bars show mean ± s.d.; *n* indicates number of cells pooled from three experiments. Scale bar, 5 μm.

peroxisomes were partially depleted from the interior of the cell. After illumination, peroxisomes remained on the cleaved side of the cell, but depletion continued on the uncleaved side. Furthermore, peroxisomes accumulated in peripheral regions, where MT plus ends are located, on the uncleaved side, as expected for kinesin-mediated transport (**Fig. 1e,f**)[16]. These results demonstrate that organelle transport induced by dimerization can be arrested with spatial and temporal control by photocleaving the dimerizer.

Activating and silencing the spindle checkpoint

To test our ability to manipulate kinetochores, we first focused on the spindle checkpoint. The checkpoint is initially active when checkpoint proteins localize to kinetochores early in mitosis, and then silenced when these proteins are removed from all kinetochores at metaphase, leading to anaphase onset. Using TNH, we aimed to control both checkpoint activation and silencing by manipulating kinetochore localization of the checkpoint protein Mad1 (**Fig. 2a**). For these experiments we used cells expressing mCherry-eDHFR-Mad1 together with Mis12-GFP-Halo or Halo-GFP-CENP-T, which are both constitutive kinetochore proteins. After adding TNH, Mad1 was recruited from the cytosol to metaphase kinetochores, and the spindle checkpoint was re-activated as <10% of cells proceeded to anaphase within 30 min. In comparison, >80% of control cells, which either did not express mCherry-eDHFR-Mad1 or were not treated with TNH, entered anaphase (**Fig. 2b**,**c**,**f**). This re-activation is consistent with previous observations using rapamycin-induced dimerization[18,19]. Rapamycin is irreversible on the relevant time scale, but we could release Mad1 from kinetochores with light by cleaving TNH. Mad1 was undetectable at kinetochores after irradiation with 405 nm light, and >80% of cells proceeded to anaphase within 30 min (**Fig. 2d**,**f**). To show spatial control, we released Mad1 from most, but not all, of the metaphase kinetochores, and cells remained arrested in metaphase (**Fig. 2e**,**f**), indicating that Mad1 localization to a few kinetochores is sufficient for checkpoint activity. Together, these results demonstrate control of both checkpoint activation and silencing.

CENP-E transports chromosomes to the spindle equator

During chromosome congression, kinetochores that initially make lateral attachments to MTs are transported to the spindle poles by cytoplasmic dynein, a minus-end-directed motor. The plus-end-directed kinetochore motor CENP-E then transports those chromosomes from the poles to the equator[20]. Successful congression depends on the ability of CENP-E to transport chromosomes selectively toward the plus ends of spindle MTs facing the equator, but not toward the plus ends of astral MTs facing the cortex, whereas polar ejection forces transport chromosomes in random directions[21]. To determine whether this directional preference is a special property of CENP-E, we tested whether a plus-end-directed motor that is not normally found at kinetochores, kinesin-1, can selectively transport chromosomes from the poles to the equator (**Fig. 3a**). For this experiment we used cells expressing Halo-GFP-SPC25, a constitutive kinetochore protein, together with K560-mCherry-eDHFR, the constitutively active motor domain of kinesin-1, as used previously[16]. We treated cells with a small-molecule CENP-E inhibitor, GSK923295, which results in accumulation of some chromosomes at the poles[22], and then recruited kinesin-1 to kinetochores by uncaging CTH at one pole (**Fig. 3b**, yellow region). Chromosomes moved away from this pole, whereas chromosomes at the unilluminated pole, serving as an internal control, showed little directional movement. The dynein–dynactin complex remains on kinetochores after kinesin-1 recruitment, indicating that the observed movement is not due to loss of dynein (**Supplementary Fig. 3**). Because kinetochore-bound Halo-GFP-SPC25 exchanges with the cytoplasmic pool, kinesin-1 that was recruited to kinetochores at the uncaged pole gradually spread to other kinetochores that were not initially targeted, leading to small displacements of those kinetochores at longer time points. Nevertheless, it is clear that kinesin-1 transported chromosomes in all directions without preference for MTs directed toward the metaphase plate (**Fig. 3c**–**e**).

To test whether CENP-E selectively transports chromosomes from poles to the equator in this assay, we recruited the CENP-E motor domain rather than kinesin-1. Because the CENP-E inhibitor would prevent activity of the recruited CENP-E motors, we knocked down endogenous CENP-E with small interfering RNA (siRNA) that does not target our recruited motors. We designed two truncated CENP-E constructs that include the motor domain and parts of the coiled-coil domain (1–467 and 1–620 amino acids). Because these constructs lack the kinetochore binding site, they were freely diffusing in the cytosol before recruitment, and some chromosomes

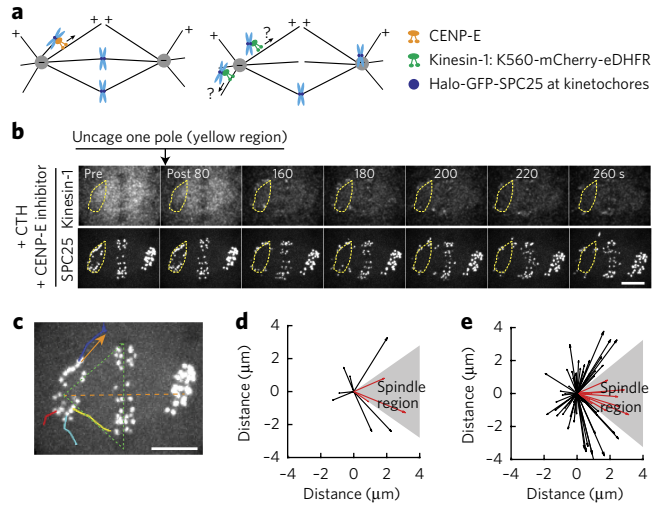

Figure 3 | Kinesin-1 transports chromosomes in all directions from the pole. (**a**) Model for CENP-E transporting pole-proximal chromosomes specifically toward the equator (left), and experimental design (right) to test whether kinesin-1, another plus-end-directed motor, can rescue CENP-E inhibition in cells expressing Halo-GFP-SPC25 and K560-mCherry-eDHFR (kinesin-1). (**b**–**e**) Cells were treated with the CENP-E inhibitor GSK923295 and CTH. CTH was then uncaged at one pole (**b**, yellow region) to recruit kinesin-1 motors to kinetochores at that pole, and cells were imaged live for 10 min. Solid lines (**c**) are representative trajectories of kinetochore movements for the cell shown in **b**. For each kinetochore, a direction vector was estimated by linking the start and end points (for example, orange arrow). The pole–pole axis (orange dashed line) and the spindle region (dashed green triangle) were drawn manually. Direction vectors are plotted for kinetochore movements at the uncaged pole in a single cell (**d**, corresponding to cell shown in **b** and **c**) and for multiple cells (**e**, n = 75 kinetochore pairs from 9 cells). The pole–pole axis is the horizontal axis, and starting points for each kinetochore are superimposed at the origin. Red arrows represent movement toward the metaphase plate. Scale bars, 5 μm.

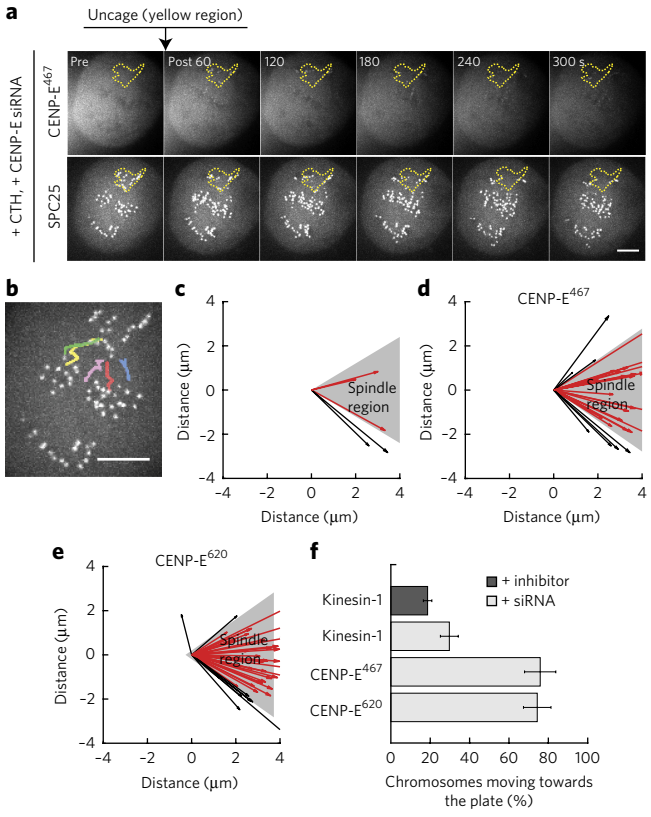

Figure 4 | CENP-E transports chromosomes from the pole to the equator. (**a**–**e**) Cells expressing Halo-GFP-SPC25 and CENP-E^{467}-mCherry-eDHFR (**a**–**d**) or CENP-E^{620}-mCherry-eDHFR (**e**) were treated with CENP-E siRNA and CTH. CTH was uncaged at one pole (yellow region), and cells were imaged live for 10 min. (**b**) Solid lines are representative trajectories of kinetochore movements for the cell shown in **a**. Direction vectors are plotted as in **Figure 3** for kinetochore movements at the uncaged pole in a single cell (**c**, corresponding to cell shown in **a** and **b**) and for multiple cells (**d**, n = 29 kinetochore pairs from 12 cells; **e**, n = 39 kinetochores pairs from 14 cells). Scale bars, 5 μm. (**f**) Percent of chromosomes moving toward the metaphase plate after recruitment of kinesin-1 or CENP-E, with endogenous CENP-E inhibited either with the inhibitor GSK923295 (data from **Fig. 3e**) or by siRNA (data from **Fig. 4d**,**e** and **Supplementary Fig. 4d**). Error bars show mean ± s.d.

accumulated at the spindle poles as with the CENP-E inhibitor. After recruitment to kinetochores, each CENP-E construct transported chromosomes predominantly from the poles to the equator (**Fig. 4**). In contrast, kinesin-1 transported chromosomes equally in all directions (**Supplementary Fig. 4**), as seen in our previous experiment with the CENP-E inhibitor (**Fig. 3**). These results demonstrate that directional congression is a specialized property of CENP-E.

CENP-E maintains chromosomes at the metaphase plate

After transporting chromosomes to the equator, CENP-E remains at kinetochores, suggesting an additional role at bi-oriented kinetochores[23]. Indeed, after CENP-E deletion or depletion, bi-oriented kinetochores bind only half the normal number of MTs, and kinetochores are more frequently attached laterally than by their ends to MTs[24,25]. In addition, CENP-E inhibition at metaphase with GSK923295 leads to chromosome movement toward the poles, which may reflect transport by poleward MT flux, because the inhibitor generates a rigor state in which CENP-E is bound to the MT but is inactive[22,26]. *In vitro*, CENP-E converts from a lateral transporter into a MT tip tracker after reaching the MT end, and maintains association with both assembling and disassembling MT tips[26]. If the tip-tracking activity contributes to CENP-E function *in vivo*, we predict that CENP-E would stabilize attachments between kinetochores and dynamic MT ends to maintain chromosome alignment at metaphase. To test this prediction, we established an assay to probe the stability of metaphase alignment by recruiting kinesin-1 to kinetochores to generate directional forces (**Fig. 5a**). After recruiting kinesin-1 to metaphase kinetochores, the metaphase plate was mildly disturbed, as the average distance of kinetochores to the equator increased slightly over time compared to a stable metaphase plate in a control experiment in which no motor was recruited (**Fig. 5b–d**). CENP-E inhibition generated some polar chromosomes, but those aligned at the metaphase plate maintained their positions over the time course of our experiment (10 min). In contrast, after recruiting kinesin-1 to kinetochores under CENP-E inhibition, chromosomes at the metaphase plate rapidly lost alignment as the average distance of kinetochores to the equator increased dramatically (**Fig. 5b–d**). This result indicates that after inhibiting CENP-E, the metaphase plate is less stable and therefore more prone to disruption by forces generated by recruited motors.

DISCUSSION

We developed new optogenetic tools and applied them to control important kinetochore functions: spindle checkpoint signaling and motor activity. The first new molecule, CTH, has a red-shifted

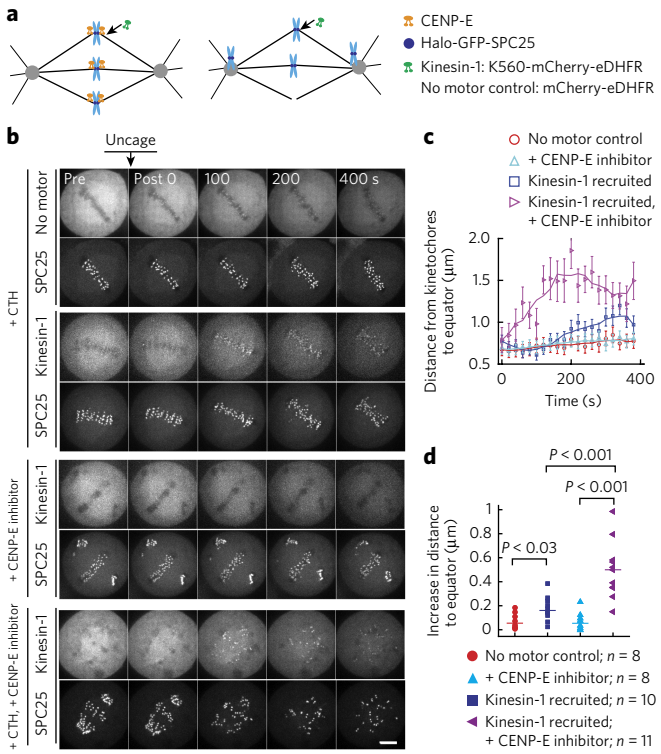

Figure 5 | CENP-E stabilizes metaphase alignment. (**a**) Experimental design to test whether CENP-E is necessary to maintain metaphase alignment by recruiting kinesin-1 motors to kinetochores in cells expressing Halo-GFP-SPC25 and K560-mCherry-eDHFR (kinesin-1), with (right) or without (left) inhibition of CENP-E. (**b**–**d**) Cells were treated with CTH and/or CENP-E inhibitor as indicated. CTH was uncaged at $t = 0$ to recruit K560-mCherry-eDHFR (or mCherry-eDHFR as a control) to all kinetochores. (**c**) Mean distances of kinetochores to the equator over time are plotted for single cells (corresponds to cells shown in **b**), with moving averages shown as solid lines ($n = 30$ kinetochores for control; $n = 38$ for CENP-E inhibitor; $n = 45$ for kinesin-1 recruited; $n = 16$ for kinesin-1 recruited with CENP-E inhibitor; error bars represent mean ± s.e.m.). (**d**) To compare data from multiple cells, mean distance was averaged over the 300–400 s time window, and the mean distance at $t = 0$ was subtracted. Each data point represents a single cell, n indicates number of cells; horizontal line, mean. P values are from two-sided t-tests. Scale bar, 5 μm.

photocage, expanding the range of wavelengths that can be used for uncaging, and requires less light to uncage compared to our previously reported NTH. The second new molecule, TNH, offers spatiotemporal control over reversal of dimerization. Our system has both advantages and disadvantages compared to photosensitive protein dimerization systems. For example, the TULIP system does not provide controlled reversibility, but rather relies on the dissociation kinetics of the protein–protein interaction[27]. The phytochrome B-phytochrome-interacting factor system can be switched on and off repeatedly using different wavelengths of light, but was not successful in targeting kinetochores[28,29]. With our system, light can be used to either trigger dimerization or reverse dimerization, depending on the choice of dimerizer, but cannot be employed for repeated ON–OFF cycles. The modular design supports further expansion, however, through creation of new dimerizers with additional properties. For example, one future goal is to combine the orthogonal coumarin photocage and NVOC linker to create a molecule that allows spatiotemporal control for both dimerization and reversal of dimerization.

Previous experiments targeting Mad1 to kinetochores showed that the checkpoint is activated by either constitutive tethering or rapamycin-induced recruitment[18,19,30], but the effects of removing Mad1 could not be examined because the targeting was not reversible. Our results show that cells progress to anaphase after removal of Mad1 from kinetochores by TNH cleavage, thus providing control over cell cycle progression through both activation and silencing of the spindle checkpoint. During normal mitotic progression, checkpoint activity is sustained as long as checkpoint proteins remain on one or a few unattached kinetochores. Our results show that maintaining Mad1, specifically, on a few kinetochores is sufficient to maintain checkpoint activity. A future goal is to test whether Mad1 localization to a single kinetochore is sufficient to activate the checkpoint, which is technically challenging because we have not yet identified a stable Halo-tagged anchor protein at kinetochores that does not exchange with the cytosolic pool for the duration of the experiment (>30 min).

Our findings reveal two specialized properties of CENP-E at kinetochores. First, we show in live cells that CENP-E transports chromosomes from poles to the equator, whereas kinesin-1 has no directional preference. This directional transport is consistent with recent findings that a post-translational modification of tubulin, detyrosination, differentiates spindle MTs that are pointing toward the equator from astral MTs, and that CENP-E prefers detyrosinated MTs[31]. Our finding that kinesin-1 does not display a similar preference for spindle microtubules is consistent with *in vitro* findings that kinesin-1 is slightly less processive on detyrosinated MTs[32], although conflicting results have also been reported in neurons[33–35]. Thus, CENP-E specifically recognizes a MT code to guide chromosome congression. Second, we show that CENP-E stabilizes metaphase alignment. Given previous findings that CENP-E tracks dynamic MT tips *in vitro*[26], our results *in vivo* indicate that CENP-E acts as a tether that can prevent kinesin-1 from walking kinetochores off the end of the MT and disrupting the metaphase configuration. Many chromosomes remain aligned after depletion or inhibition of CENP-E[25,26,36], likely because other MT-binding proteins at kinetochores can maintain MT attachment. Our results indicate that kinetochores lacking CENP-E are more vulnerable to perturbations, however, such as those introduced by our kinesin-1 recruitment. Overall, our results support a two-step model in which CENP-E transports kinetochores to MT plus ends during congression and then maintains attachment of bi-oriented sister kinetochores to MT ends during metaphase oscillations.

This work establishes a foundation for optogenetic control of kinetochore function and highlights the advantages of a hybrid chemical and genetic approach. We are able to manipulate both gain and loss of enzymatic activities using light, with flexibility provided by the choice of proteins to tag and the choice of probes. We envision our approach to be readily adapted to probe other kinetochore processes, such as regulation by kinases and phosphatases, tension sensing and MT capture[37–39]. Our optogenetic tools are also broadly applicable to experimentally probe other dynamic cellular processes that depend on spatiotemporal regulation of protein localization.

Received 15 February 2017; accepted 17 July 2017;
published online 14 August 2017

METHODS

Methods, including statements of data availability and any associated accession codes and references, are available in the online version of the paper.

References

1. Nagpal, H. & Fukagawa, T. Kinetochore assembly and function through the cell cycle. *Chromosoma* **125**, 645–659 (2016).
2. Pesenti, M.E., Weir, J.R. & Musacchio, A. Progress in the structural and functional characterization of kinetochores. *Curr. Opin. Struct. Biol.* **37**, 152–163 (2016).

3. Cheeseman, I.M. The kinetochore. *Cold Spring Harb. Perspect. Biol.* **6**, a015826 (2014).
4. Holland, A.J. & Cleveland, D.W. Losing balance: the origin and impact of aneuploidy in cancer. *EMBO Rep.* **13**, 501–514 (2012).
5. Walczak, C.E., Cai, S. & Khodjakov, A. Mechanisms of chromosome behaviour during mitosis. *Nat. Rev. Mol. Cell Biol.* **11**, 91–102 (2010).
6. Auckland, P. & McAinsh, A.D. Building an integrated model of chromosome congression. *J. Cell Sci.* **128**, 3363–3374 (2015).
7. Lara-Gonzalez, P., Westhorpe, F.G. & Taylor, S.S. The spindle assembly checkpoint. *Curr. Biol.* **22**, R966–R980 (2012).
8. London, N. & Biggins, S. Signalling dynamics in the spindle checkpoint response. *Nat. Rev. Mol. Cell Biol.* **15**, 736–747 (2014).
9. Goshima, G. & Vale, R.D. The roles of microtubule-based motor proteins in mitosis: comprehensive RNAi analysis in the *Drosophila* S2 cell line. *J. Cell Biol.* **162**, 1003–1016 (2003).
10. Lampson, M.A. & Kapoor, T.M. Unraveling cell division mechanisms with small-molecule inhibitors. *Nat. Chem. Biol.* **2**, 19–27 (2006).
11. Magidson, V., Lončarek, J., Hergert, P., Rieder, C.L. & Khodjakov, A. Laser microsurgery in the GFP era: a cell biologist's perspective. *Methods Cell Biol.* **82**, 239–266 (2007).
12. Toettcher, J.E., Voigt, C.A., Weiner, O.D. & Lim, W.A. The promise of optogenetics in cell biology: interrogating molecular circuits in space and time. *Nat. Methods* **8**, 35–38 (2011).
13. van Bergeijk, P., Adrian, M., Hoogenraad, C.C. & Kapitein, L.C. Optogenetic control of organelle transport and positioning. *Nature* **518**, 111–114 (2015).
14. Jost, A.P.-T. & Weiner, O.D. Probing yeast polarity with acute, reversible, optogenetic inhibition of protein function. *ACS Synth. Biol.* **4**, 1077–1085 (2015).
15. Ballister, E.R., Aonbangkhen, C., Mayo, A.M., Lampson, M.A. & Chenoweth, D.M. Localized light-induced protein dimerization in living cells using a photocaged dimerizer. *Nat. Commun.* **5**, 5475 (2014).
16. Ballister, E.R., Ayloo, S., Chenoweth, D.M., Lampson, M.A. & Holzbaur, E.L.F. Optogenetic control of organelle transport using a photocaged chemical inducer of dimerization. *Curr. Biol.* **25**, R407–R408 (2015).
17. Klán, P. *et al.* Photoremovable protecting groups in chemistry and biology: reaction mechanisms and efficacy. *Chem. Rev.* **113**, 119–191 (2013).
18. Ballister, E.R., Riegman, M. & Lampson, M.A. Recruitment of Mad1 to metaphase kinetochores is sufficient to reactivate the mitotic checkpoint. *J. Cell Biol.* **204**, 901–908 (2014).
19. Kuijt, T.E.F., Omerzu, M., Saurin, A.T. & Kops, G.J.P.L. Conditional targeting of MAD1 to kinetochores is sufficient to reactivate the spindle assembly checkpoint in metaphase. *Chromosoma* **123**, 471–480 (2014).
20. Kapoor, T.M. *et al.* Chromosomes can congress to the metaphase plate before biorientation. *Science* **311**, 388–391 (2006).
21. Barisic, M., Aguiar, P., Geley, S. & Maiato, H. Kinetochore motors drive congression of peripheral polar chromosomes by overcoming random arm-ejection forces. *Nat. Cell Biol.* **16**, 1249–1256 (2014).
22. Wood, K.W. *et al.* Antitumor activity of an allosteric inhibitor of centromere-associated protein-E. *Proc. Natl. Acad. Sci. USA* **107**, 5839–5844 (2010).
23. Cooke, C.A., Schaar, B., Yen, T.J. & Earnshaw, W.C. Localization of CENP-E in the fibrous corona and outer plate of mammalian kinetochores from prometaphase through anaphase. *Chromosoma* **106**, 446–455 (1997).
24. Shrestha, R.L. & Draviam, V.M. Lateral to end-on conversion of chromosome-microtubule attachment requires kinesins CENP-E and MCAK. *Curr. Biol.* **23**, 1514–1526 (2013).
25. Putkey, F.R. *et al.* Unstable kinetochore-microtubule capture and chromosomal instability following deletion of CENP-E. *Dev. Cell* **3**, 351–365 (2002).
26. Gudimchuk, N. *et al.* Kinetochore kinesin CENP-E is a processive bi-directional tracker of dynamic microtubule tips. *Nat. Cell Biol.* **15**, 1079–1088 (2013).
27. Strickland, D. *et al.* TULIPs: tunable, light-controlled interacting protein tags for cell biology. *Nat. Methods* **9**, 379–384 (2012).
28. Yang, X., Jost, A.P.-T., Weiner, O.D. & Tang, C. A light-inducible organelle-targeting system for dynamically activating and inactivating signaling in budding yeast. *Mol. Biol. Cell* **24**, 2419–2430 (2013).
29. Levskaya, A., Weiner, O.D., Lim, W.A. & Voigt, C.A. Spatiotemporal control of cell signalling using a light-switchable protein interaction. *Nature* **461**, 997–1001 (2009).
30. Maldonado, M. & Kapoor, T.M. Constitutive Mad1 targeting to kinetochores uncouples checkpoint signalling from chromosome biorientation. *Nat. Cell Biol.* **13**, 475–482 (2011).
31. Barisic, M. *et al.* Mitosis. Microtubule detyrosination guides chromosomes during mitosis. *Science* **348**, 799–803 (2015).
32. Sirajuddin, M., Rice, L.M. & Vale, R.D. Regulation of microtubule motors by tubulin isotypes and post-translational modifications. *Nat. Cell Biol.* **16**, 335–344 (2014).
33. Dunn, S. *et al.* Differential trafficking of Kif5c on tyrosinated and detyrosinated microtubules in live cells. *J. Cell Sci.* **121**, 1085–1095 (2008).
34. Konishi, Y. & Setou, M. Tubulin tyrosination navigates the kinesin-1 motor domain to axons. *Nat. Neurosci.* **12**, 559–567 (2009).
35. Hammond, J.W. *et al.* Posttranslational modifications of tubulin and the polarized transport of kinesin-1 in neurons. *Mol. Biol. Cell* **21**, 572–583 (2010).
36. McEwen, B.F. *et al.* CENP-E is essential for reliable bioriented spindle attachment, but chromosome alignment can be achieved via redundant mechanisms in mammalian cells. *Mol. Biol. Cell* **12**, 2776–2789 (2001).
37. Heald, R. & Khodjakov, A. Thirty years of search and capture: The complex simplicity of mitotic spindle assembly. *J. Cell Biol.* **211**, 1103–1111 (2015).
38. Lampson, M.A. & Grishchuk, E.L. Mechanisms to avoid and correct erroneous kinetochore-microtubule attachments. *Biology (Basel)* **6**, 1 (2017).
39. Funabiki, H. & Wynne, D.J. Making an effective switch at the kinetochore by phosphorylation and dephosphorylation. *Chromosoma* **122**, 135–158 (2013).

Acknowledgments

We thank G. Furst and J. Gu for NMR assistance; R. Kohli for High-Resolution Mass Spectrometry (HRMS) assistance; A. Calderon and A. Gokden for assistance with molecular cloning and generating cell lines; D. Cleveland (University of California at San Diego) and E. Grishchuk (University of Pennsylvania) for CENP-E plasmids, L. Lavis for dye JF585 (Janelia Research Campus, HHMI); and E. Grishchuk and members of the Lampson lab for helpful discussions. C.A. thanks the Royal Thai Government for PhD fellowship funding through the Development and Promotion of Science and Technology (DPST) Project. This work was supported by the US National Institutes of Health (GM083988 to M.A.L. and GM118510 to D.M.C.) and the US National Institutes of Health, National Cancer Institute (U54-CA193417).

Author contributions

H.Z. designed and conducted biological experiments and wrote the manuscript. C.A. synthesized and characterized the dimerizers, conducted experiments in **Figure 1** and **Supplementary Figures 1** and **2** and edited the manuscript. E.V.T. conducted experiments in **Figure 4** and **Supplementary Figure 4**. E.R.B. contributed to the design of dimerizers and checkpoint experiments. D.M.C. and M.A.L. designed experiments and edited the manuscript.

Competing financial interests

The authors declare no competing financial interests.

Additional information

Any supplementary information, chemical compound information and source data are available in the online version of the paper. Reprints and permissions information is available online at http://www.nature.com/reprints/index.html. Publisher's note: Springer Nature remains neutral with regard to jurisdictional claims in published maps and institutional affiliations. Correspondence and requests for materials should be addressed to M.A.L. or D.M.C.

ONLINE METHODS

Dimerizer synthesis, characterization and storage. Details of dimerizer synthesis and characterization with NMR spectra are in **Supplementary Note 1**. Dimerizers were dissolved in DMSO at 10 mM and stored in amber plastic microcentrifuge tubes at −80 °C for long-term storage. For experiments, an aliquot was diluted in cell culture medium to final working concentration (10 μM for CTH and 100 nM for TNH, unless otherwise stated) and kept at −20 °C, then warmed to 37 °C when ready to use. Care was taken to minimize exposure of dimerizers to light and heat before experiments. Working quickly in normal room lighting, or low levels of white light used for differential interference contrast microscopy, did not cause detectable premature cleavage of TNH or uncaging of CTH.

Plasmids. All plasmids in this study are derived from pEM705, which contains a CAG promoter for constitutive expression, obtained from E.V. Makeyev (Nanyang Technological University, Singapore)[40]. Plasmid 764: Halo-GFP-ActA includes the C-terminal 47 amino acids of the *Listeria monocytogenes* ActA gene, which confer mitochondrial outer membrane targeting. Plasmid 775: PEX3-GFP-Halo includes the N-terminal 42 amino acids of the human Pex3 gene, which confer peroxisome targeting. Plasmid 767: KLC1-mCherry-eDHFR includes residues 1–175 of rat kinesin-1 light chain. Plasmid 768: K560-mCherry-eDHFR includes residues 1–560 of human kinesin-1 heavy chain. Plasmid 770: BICD-mCherry-eDHFR includes residues 1–572 of mouse BICD2. Plasmids 764, 767, 768, 770, and 775 were previously reported[15,16]. Plasmid 850: Halo-GFP-CENP-T contains the full length human kinetochore protein CENP-T. Plasmid 858: 3× Halo-GFP-SPC25 has three Haloenzymes fused to full length human kinetochore protein SPC25. Plasmid 841: mCherry-eDHFR-Mad1 was made by inserting Mad1 into plasmid 752: mCherry-eDHFR. CENP-E^{620} and CENP-E^{467} are truncations of human CENP-E (residues 1–620 or 1–467), which based on sequence contain the motor domain and a short part of the coiled-coil region but lack a substantial part of the stalk, the kinetochore binding domain, and the second MT binding site[41,42]. CENP-E^{467}-mCherry-eDHFR and CENP-E^{620}-mCherry-eDHFR were derived from plasmid 768: K560-mCherry-eDHFR. The CENP-E^{620} cDNA with nucleotide sequence optimized for *E. coli* was amplified using PCR to generate CENP-E^{620} and CENP-E^{467}.

Cell culture and cell lines. All experiments were performed with HeLa acceptor cells as previously described[15], originally obtained from E.V. Makeyev, Nanyang Technological University, Singapore[40]. Cells were cultured in growth medium (Dulbecco's modified Eagle's medium with 10% FBS and 1% penicillin–streptomycin) at 37 °C in a humidified atmosphere with 5% CO_2. The cell line stably expressing Haloenzyme fused to CENP-B in **Supplementary Figure 1a** was reported previously[15]. All kinetochore experiments were performed with Haloenzyme-tagged kinetochore proteins (Mis12, SPC25 and CENP-T) stably expressed in cell lines. The eDHFR constructs (Mad1 or motor proteins) were transiently expressed by transfection with Lipofectamine 2000 (Invitrogen) 24 h before imaging following the manufacturer's protocol. Transfections for **Figure 1** and **Supplementary Figure 1** were with a ratio of 1 μg plasmid DNA to 6 μL of FuGene 6 (Promega) 40 h before the experiment. The Mis12-GFP-Halo cell line was created using CRISPR–Cas 9 to tag the endogenous Mis12 with Haloenzyme and GFP[43], and GFP-positive cells were sorted with flow cytometry. Guide RNAs used for Mis12 are CACCGTTAATTGCTCAGTAGTCAAA and AAACTTTGACTACTGAGCAATTAAC. Halo-GFP-CENP-T and Halo-GFP-SPC25 cell lines were created using the HILO recombinase-mediated cassette exchange system (obtained from E.V. Makeyev, Nanyang Technological University, Singapore)[40]. Briefly, HeLa acceptor cells at 60–80% confluency in a well of a six-well plate were transfected with 1 μg of Halo-GFP-SPC25 or Halo-GFP-CENP-T plasmid together with 10 ng of a Cre recombinase plasmid using Lipofectamine 2000. Two days after transfection, 1 μg/mL puromycin was added to the growth medium to select stable cell lines. After selection, the top 5% of Halo-GFP-SPC25 positive cells were sorted and collected with flow cytometry. For CENP-E siRNA, cells were cotransfected with CENP-E siRNA[44] together with K560-mCherry-eDHFR, CENP-E^{467}-mCherry-eDHFR, or CENP-E^{620}-mCherry-eDHFR. Cells at ~60–80% confluency in one well of a 6-well plate were transfected with 1 μg of plasmid DNA and 2 μg of siRNA using 5 μL Lipofectamine 2000. Experiments were performed 24–48 h after transfection. Hoechst staining was used to verify absence of bacterial contamination.

Dimerizer cytotoxicity assay. AlamarBlue (Molecular Probes, catalog no. DAL1100) cell viability assays were performed following the protocol provided by the manufacturer (Thermo Fisher Scientific). The assay is based on conversion of a water-soluble dye, resazurin, into a fluorescent and colorimetric indicator by metabolically active cells. Damaged and nonviable cells generate lower signal due to reduced metabolic activity. HeLa cells expressing Halo-GFP-Spc25 were cultured in a 96-well assay plate (Corning Incorporated Costar, 3603), ~1×10^4 cells per well. Cells were treated with CTH or TNH, or with DMSO or Blasticidin S HCl (10 μg/mL; Thermo Fisher Scientific, catalog no. A1113903) as controls. The final DMSO concentration was kept at 0.5% in 100 μL media in each well. After incubating with the dimerizers for 24 h, cells were washed once with 200 μL of fresh DMEM, then incubated with the AlamarBlue reagent (10× dilution in DMEM medium) for 2 h to allow conversion of resazurin to resorufin. The fluorescence signal was measured at 37 °C with 550 nm excitation and 590 nm emission wavelengths, using a Tecan plate reader (model, Infinite M1000 PRO) operated by Tecan i-control software. The fluorescence signal was background subtracted based on wells without cells and calculated as a percentage of the signal from DMSO control cells. Each dimerizer concentration was tested in quadruplicate, and data were averaged over three independent experiments.

Image acquisition. For live imaging, cells were seeded on 22 × 22 mm glass coverslips (no. 1.5; Fisher Scientific) coated with poly-D-lysine (Sigma-Aldrich) in single wells of a six-well plate. When ready for imaging, coverslips were mounted in magnetic chambers (Chamlide CM-S22-1, LCI) with cells maintained in L-15 medium without phenol red (Invitrogen) supplemented with 10% FBS and 1% penicillin–streptomycin at 37 °C on a heated stage in an environmental chamber (Incubator BL; PeCon GmbH). Images were acquired with a spinning disk confocal microscope (DM4000; Leica) with a ×100 1.4 NA objective, an XY Piezo-Z stage (Applied Scientific Instrumentation), a spinning disk (Yokogawa), an electron multiplier charge-coupled device camera (ImageEM; Hamamatsu Photonics), and a laser merge module equipped with 488- and 593-nm lasers (LMM5; Spectral Applied Research) controlled by MetaMorph software (Molecular Devices). For Mad1 experiments, time series were taken with time interval and duration manually decided based on cell cycle progression, and z-stacks for both GFP and mCherry channel were taken with 0.5 μm spacing for a total of 3 μm. For motor experiments, time series were taken with a time interval of 20 s for total of 10 min, and z-stacks for both GFP and mCherry channel were taken with 0.5 μm spacing for a total of 5 μm, or in some cases (**Fig. 4** and **Supplementary Fig. 4**), 0.5–0.75 μm spacing for 15 steps. mCherry images in some cases (**Fig. 4** and **Supplementary Fig. 4**) were obtained less frequently, with a time interval of 60–120 s.

Dimerization and photo-activation. For CTH experiments, cells were incubated with 10 μM CTH for 1 h, which was followed by a 30-min washout to remove unbound CTH. For TNH experiments, 100 nM TNH was added directly to cells on the microscope stage. Targeted uncaging or cleavage was performed with an iLas2 illuminator system (Roper Scientific), equipped with a 405-nm laser (CrystaLaser LC, model # DL405-050-O; output of 27 mW after fiber coupling) controlled using the iLas2 software module within MetaMorph. For whole-cell UV exposure experiments (**Fig. 1c**), light from a mercury arc lamp (Osram HXP R 120W/45C Vis) was filtered through a 387/11 nm band pass filter (Semrock, part # FF01-387/11 as a component in a DAPI filter cube) and focused through the objective. For targeted irradiation with the 405-nm laser, a region of interest was defined using MetaMorph. 7% laser power and 20 repetitions were used for CTH activation, and 8% laser power and 40 repetitions were used for TNH cleavage unless otherwise stated. The CENP-E inhibitor GSK923295 (Cayman Chemical Company) was used at 50 nM and added to cells together with CTH and kept in the medium during CTH washout and imaging.

Statistical analyses. *P* values in **Figure 5d** are from two-sided *t*-tests.

Image processing. Images were processed with ImageJ[45]. All images shown are maximum-intensity projections from all slices in z-stacks, except for mCherry images in **Figure 4**, which are maximum-intensity projections of z-sections with visible mCherry to improve the signal-to-noise ratio. For **Figures 3** and **4**, kinetochore pairs were manually tracked to locate the start and end points of movement, and direction vectors were estimated by linking the start and end points. The pole-to-pole axis was defined by manually drawing a line perpendicular to the metaphase plate through the two pole regions. The spindle region was drawn manually by linking the pole and the edges of the metaphase plate. Coordinates were imported into MATLAB (MathWorks), and the angle between the direction of kinetochore movement and the pole-to-pole axis was calculated and plotted by placing the origin of movement at the origin of the coordinate plane, with the pole-to-pole axis as the horizontal axis. For quantification in **Figure 5**, cells of interest in the Halo-GFP-SPC25 channel were cropped out from a maximum projection image and registered using the plugin StackReg with scaled rotation. The equator was estimated by manually drawing a line through the kinetochores at the first time point. For cells with CENP-E inhibitor, a region was drawn to include kinetochores at the equator and exclude those at the poles at the first time point, and only kinetochores in this region were analyzed for the following time points. Kinetochore coordinates were obtained by finding maxima in ImageJ and imported into MATLAB to calculate the average distance to the equator at each time point. Moving averages (**Fig. 5d**) were obtained with the smooth function in MATLAB.

Data availability. All data generated during this study are included in this article and/or the associated supplementary information. Our research resources, including protocols, cells, and dimerizers are available upon reasonable request. The corresponding authors adhere to the NIH Grants Policy and Sharing of Unique Research Resources.

40. Khandelia, P., Yap, K. & Makeyev, E.V. Streamlined platform for short hairpin RNA interference and transgenesis in cultured mammalian cells. *Proc. Natl. Acad. Sci. USA* **108**, 12799–12804 (2011).
41. Yen, T.J., Li, G., Schaar, B.T., Szilak, I. & Cleveland, D.W. CENP-E is a putative kinetochore motor that accumulates just before mitosis. *Nature* **359**, 536–539 (1992).
42. Liao, H., Li, G. & Yen, T.J. Mitotic regulation of microtubule cross-linking activity of CENP-E kinetochore protein. *Science* **265**, 394–398 (1994).
43. Ran, F.A. *et al.* Genome engineering using the CRISPR-Cas9 system. *Nat. Protoc.* **8**, 2281–2308 (2013).
44. Johnson, V.L., Scott, M.I.F., Holt, S.V., Hussein, D. & Taylor, S.S. Bub1 is required for kinetochore localization of BubR1, Cenp-E, Cenp-F and Mad2, and chromosome congression. *J. Cell Sci.* **117**, 1577–1589 (2004).
45. Schneider, C.A., Rasband, W.S. & Eliceiri, K.W. NIH Image to ImageJ: 25 years of image analysis. *Nat. Methods* **9**, 671–675 (2012).

doi:10.1038/nchembio.2456